International Journal of
INTELLIGENT SYSTEMS AND APPLICATIONS IN ENGINEERING
ISSN:2147-6799 www.ijisae.org Original Research Paper

Retinal Glaucoma Detection Using Deep Learning Algorithm

Tanya Maurya[1], Lalitha Kala[2], Kaveti Manasa[3], Kanimozhi. G.*[4], Umayal. C.[5]

Submitted: 21/08/2021 Accepted : 27/012022

Abstract: Glaucomatic retinopathy is a degenerative eye disease that is assessed as it progresses, making it necessary to examine it more frequently. A novel method of analyzing retinal images by detecting vessels and exudates has been proposed to analyze retinal vascular disorders. In this work, noise removal is modified by a suitable nonlinear function. The modified function parameters are derived by using fast DCT (FDCT) coefficients, which enhance weak edges while eliminating noise. In this work, a minimum of 10 features such as Mean, Variance, Entropy with the data set trained images on 15 images using NN (neural network) training is implemented, and NN classifier based Normal or Abnormal is applied. Simulation is done using MATLAB Simulink and comparisons among Discrete Wavelet, Curvelet, Orthogonal transform, and fuzzy segmentation are executed and the blood vessels segmentation resulted in promising results. This work proposes deep learning-based system for glaucoma diagnosis using retinal fundus images, developed using image processing and deep learning approaches.

Keywords: *Curvelet, Discrete fuzzy Glaucoma, noise orthogonal Pre-processing, removal, segmentation, transform, wavelet.*

1. Introduction

One of the most frightening complications of glaucoma is the degenerative eye disease glaucoma retinopathy. There is a condition called Glaucomatous Retinopathy when a small group of blood vessels in the retina are damaged, known as capillaries. As a result of persistent non-proliferative glaucomatic retinopathy (NPDR), capillaries begin to swell and form microaneurysms, which are small bulges on the end of blood vessels. Over time, such microaneurysms starts leaking blood and fluid on the retina, impairing sight. According to this paper, a fresh salient based methodology to determine outflowing fluorescent dye X-ray photography. An excellent constituent approach is first of all used to break the image up into purposeful squares (or pixels) at completely different scales. 2 strikingness factors, intensity, and compact, area unit then projected to estimate the striking map every of every} individual super constituent systematically. The strikingly maps at completely different scales over a similar cues area unit consolidated victimization associate degree averaging operator. the 2 strikingly maps over completely different data area unit consolidated employing a pixel-by-pixel multiplication algorithm [10]. Leaky spots area unit identified by threshold the strikingness map and then a graph-cut segmentation as shown in Fig. 1. (a)

Applications of saliency detection in medical images uses a multi-level super element illustration as part of the pre-processing step, and the salience map is desegregated from all obtained salience maps following the colour and texture options. Through the coding and recognition of picture features, this methodology Clearly portrays the contours of ulcerous regions. The purpose of this technique is to resolve the issue of rigid methods not being able to administer effective results when there are changes in intensity. Despite the salience providing excellent sharp pics, gradient data will continue to be affect by the noise, as shown in Fig. 2.

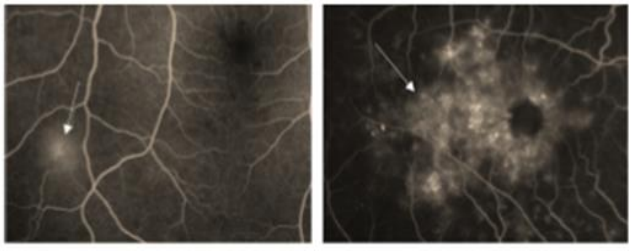

(a) (b)

Fig. 1. Figures showing two different retinal diseases with focal leakages. (a) malarial retinopathy (b) glaucomatic retinopathy.

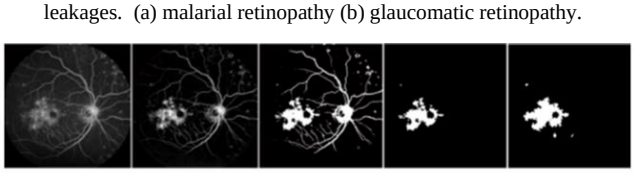

(a) (b) (c) (d) (e)

Fig. 2. Sample algorithm for detecting leakages: (a) FA images; (b) saliency maps of (a). (c) binary images of (b) derived from the threshold value T; (d) regions of leakage after masking vessel and disk regions; (e) expert's annotations.

This paper presents a supervised segmentation technique for retinal blood vessels that uses a deep neural network that is pre-processed with zero-phase lightening, and geometric transformations and

[1] *School of Electrical Engineering, VIT Chennai, Tamil Nadu, India ORCID ID :0000-0002-6504-2952*
[2] *School of Electrical Engineering, VIT Chennai, Tamil Nadu, India ORCID ID : 0000-0002-3899-8385*
[3] *School of Electrical Engineering, VIT Chennai, Tamil Nadu, India ORCID ID : 0000-0003-2351-1826*
[*] *School of Electrical Engineering, VIT Chennai, Tamil Nadu, India ORCID ID : 0000-0001-6823-3781*
[5] *School of Electrical Engineering, VIT Chennai, Tamil Nadu, India ORCID ID : 0000-0003-3757-713X*
* *Corresponding Author Email:kanimozhi.g@vit.ac.in*

gamma corrections on a large (up to four hundred) set of examples. There are several variants of the strategy, as well as structured prediction, where a network classifies multiple pixels at the same time. As applied to plain benchmarks of bodily structure imaging, the DRIVE, STARE, and CHASE databases, the networks considerably crush the previous algorithms on the world below mythical monster curve live (up to > 0.99) and accuracy of classification (up to > 0.95). Moreover, the strategy is proof against the development of the central vessel reflex, sensitive in detecting fine vessels (sensitivity >0.88) and does well in pathological cases. A convolutional neural network (CNN) is composed of multiple elementary process units. includes many weighted inputs and one output, activity convolution of input signals with weights, and reworking the result with some style of nonlinearity. Their locations in a very layer correspond to pixels in an input image. The unit arrangement is the primary characteristic that makes CNNs appropriate for the processing of visual information; the opposite options square measure native properties, parameter sharing, and pooling of hidden units. Native property means a given unit receives information solely from its receptive field (RF), a little parallelogram of image pixels (for the units within the first layer) or units within the previous layer (for the following layers) The RFs of neighbouring units in a very layer usually offset by stride.

i. **Global Contrast Normalization (GCN):** The images in Fig.3(a) indicate that the brightness variation across the FOV, to assist the educational method to abstract from these fluctuations and specialize in vessel detection.

ii. **Zero-phase part analysis (ZCA Whitening): One feature of a vessel segmentation rule is its ability to detect capillaries:** To examine these characteristics of decilitre networks, amend the manual segmentations within DRIVE information to mechanically remove the thick vessels. To accomplish the aim, tend to perform a morphological gap, discard the connected parts with area * 100 pixels, work out this image from the first manual segmentation, and take away from the resulting image the connected parts smaller than eight pixels. Fig [3](b) shows the partitions for the resulting coaching pictures [11].

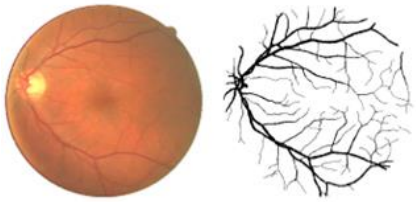

(a)

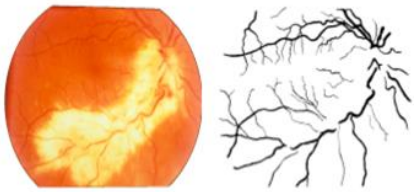

(b)

Fig. 3. (a) A training image from the DRIVE database (left) and the corresponding manual segmentation (right). (b) A pathological image from the STARE database (left) and the corresponding manual segmentation (right)

In this study, a detailed description and analysis of the methodology for vessel segmentation based on FCCRF is presented. The methodology is evaluated quantitatively and qualitatively on four publicly accessible datasets: DRIVE, STARE, CHASEDB1, and HRF.

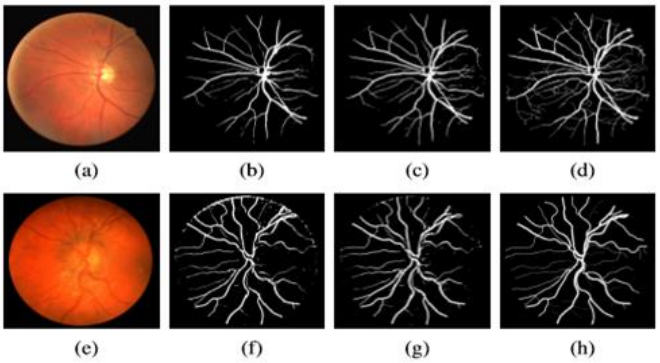

Fig. 4. Segmentation results obtained on DRIVE and CHASEDB1. (a): Image 04 of DRIVE and (e)Image_05L of CHASEDB1 (b),(f) Segmentations obtained using only the unary potentials (c) and (g) Segmentations obtained using the FCCRF model (d) and (h) Ground truth labelling

Localizing Micro Aneurysms in Fundus Images through Singular Spectrum Analysi**s:** It is necessary to recognize small aneurysms once developing an automatic analysis system for glaucomatic retinopathy detection. A singular spectrographic analysis is used to process the cross-sectional profiles in multiple directions. The correlation coefficient between every processed profile. Glaucomatous retinopathy (DR) is a small tube-shaped structure and the leading cause of vision loss amongst the working-age population [1].

Combining a supervised constituent classification with a topper-based rule to detect dark lesions in coloured body structure images. The k-nearest neighbour (k-NN) classifier was used to improve MA detection using intensity and form descriptors. In Fig [5] the detection of MAs and larger dark lesions (i.e., haemorrhages) utilizing a similar method can be seen.

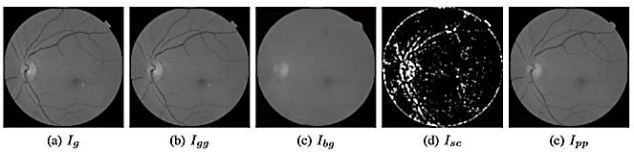

Fig. 5. (a) The green channel of the fundus image. (b) The Gaussian filtered image of (a). (c) The estimated background image Ibg. (d) Shade correction image Isc was accomplished by subtracting the median filtered image Ibg from Igg. (e) The pre-processed image Ipp.

A total of 11 features are extracted from the scaled profiles for classification, few of them are:

(1) The mean and standard deviation (_peak and *_peak) of the peak widths across all cross-section profiles of the object.

(2) The mean and standard deviation (μ_dec and σ_dec) of the heights of decreasing slopes of all cross-section profiles of the object.

(3) The mean and standard deviation (μ_inc and σ_inc) of the heights of increasing slopes of all cross-section profiles of the object.

(4) The compactness of an object is denoted as v = q(Pn j=1 dj −d)/n, where dj is the distance from its j-th edge point of slope (slope inc, slope dec) to the centroid of the profile and d is the mean of the distance from each edge point to the centroid. Here n is the total number of edge points (n = 24 in the

implementation, as each candidate has 12 profiles, each profile has two edge pixels).

(5) The mean and standard deviation (μλ1 and σλ1) of the largest eigenvalues of all profiles.

(6) The mean and standard deviation (μr and σr) of the aspect ratio, r = λ1/λ2. λ1 and λ2 are the respective values of the first and second-largest eigenvalues of a profile.

Optic Disc Boundary and Vessel Origin Segmentation of Fundus Images: In this paper, an entirely novel blind spot (OD) segmentation rule is introduced that detects the OD boundary as well as the location of the vessel origin (VO) point. In the first step, a circular structuring component is used to resize and reconstruct the inexperienced plane of each complex body part image. Having morphologically reconstructed the image, bright areas, which lie in the vicinity of closed blood vessels, are then extracted. A Gaussian Mixture Model classifier is employed to separate brilliant probable and non-OD OD regions. As the best candidate region for OD, the brightest probable OD region with the highest Vessel-Sum and Solidity is detected.

A bright alternative to the simplest candidate OD region is then detected 1 disc diameter from the center of mass as another possible candidate region. There is then a bell-shaped hull containing all the candidate OD regions, and the best-fit conic across the bell-shaped hull defines the divided OD boundary. The location of the VO enables the detection of the center of mass of major blood vessels at intervals from the divided OD boundary. There is a low-quality computation time for the projected rule, and it is strong against variations in illumination, angle of imaging, and retinal abnormalities. GD segmentation and OD overlap score achieved by the algorithm are within the range of 88.8-100% for images from DRIVE, DIARETDB1, DIARETDB0, CHASE DB1, Messidor and STARE in only 2.14 seconds per image. Thus, the projected rule will be used for machine-driven detection of retinal pathologies like eye disease, glaucomatic retinopathy, and maculopathy.

- First, a circular structuring element half the diameter of the estimated OD yields a better extraction of bright OD regions than horizontal linear elements of length equal to the estimated OD diameter.
- Secondly, identify features of bright OD regions that distinguish bright probable OD regions from bright non-OD regions by using the Gaussian Mixture Model (GMM).
- Thirdly, resizing and cross-validating retinal data sets provide an optimal training data set (TRAIN50) to distinguish bright OD regions from non-OD regions regardless of the image FOV or the degree of pathological atrophy.

(f) Retinal Disease Screening through Local Binary Patterns: This work examines the ability to distinguish between pathological and healthy images based on differences in texture within pictures of body structures. A comparison has been conducted concerning native Binary Patterns (LBP) as a texture descriptor for retinal pictures, as well as with native section division (LPQ) and LBP filtering (LBPF). SLIM measures tissue layer background to avoid the previous lesion segmentation stage and allows us to tell apart glaucomatic retinopathy (DR), age-related macular degeneration (AMD) from traditional body structure pictures. The five experiments were designed and validated with the proposed procedure showing promising results (differentiating DR from AMD, AMD from pathological, and DR from AMD).

2. Segmentation (Image Processing)

Segmentation, also known as super pixels (sets of pixels), is a computer vision technique in which data is divided into segments. [5] Segmentation aims to simplify or transform an image so that it is more meaningful and easier to analyze.[3] There are currently three ways to detect glaucoma: Edge detection methods, segmentation methods, and retinal grading algorithms.

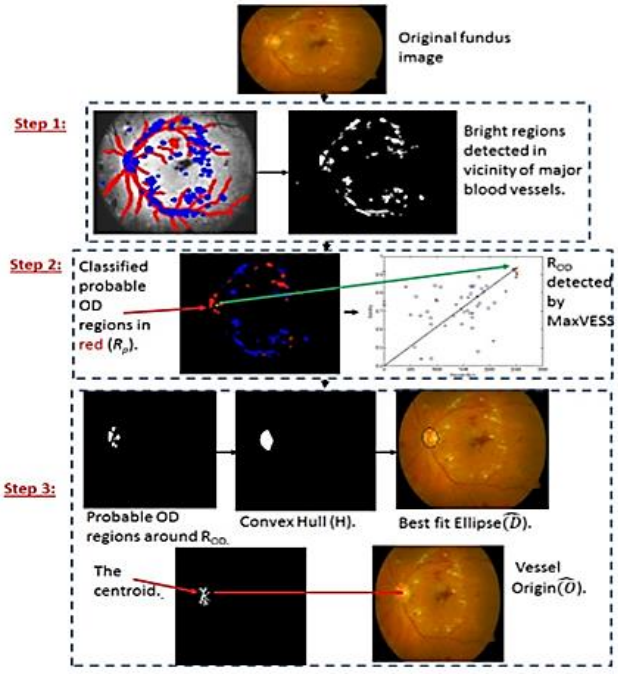

Fig. 6. 3-step automated OD and VO segmentation algorithm

(1) Histogram-based methods: These methods compute a histogram from every pixel in the image, and then use the peaks and valleys in the histogram to locate clusters within the image. Color or intensity can be used as the measure.

(2) Edge detection: The intensity at the boundary of a region adjusts sharply, so region boundaries and edges are closely related. Edge detection techniques are used as the base of another segmentation technique.

(3) Graph partitioning methods: The graph partitioning methods are effective for segmenting images. These methods model the image as a weighted, undirected graph

(4) Level set methods: They are characterized by the development of a curve towards the lowest potential of a cost function, where the function definition reflects the task to be addressed and imposes certain smoothness constraints.

(5) Multi-scale segmentation: Image segments in various scales are computed, and some are propagated from coarse to fine scales. See multi-scale segmentation.

(6) Neural networks segmentation: Neural networks segmentation uses artificial neural networks [23] to retrieve information about small areas of an image. A type of network designed especially for this is the Kohonen map.

(7) Fuzzy Logic: Based on fuzzy set theory, fuzzy logic applies to approximate rather than precise reasoning. A fuzzy logic variable may have a truth value of between 0 and 1 as opposed to binary logic variables of flashy logic, which only have two truth values, and others need to be constrained to two truth values, less accurate, and less efficient, and not suitable for all lighting conditions.

3. Proposed System

Retinal image analysis for glaucomatic retinopathy detection is based on Kirsch's template-based edge Enhancement followed by the morphological filtering, object classification with connected component analysis with the advantages of accurate retina vessel and execute detection, better efficiency, and less sensitivity to noise- it is useful to detect glaucoma in an early stage.

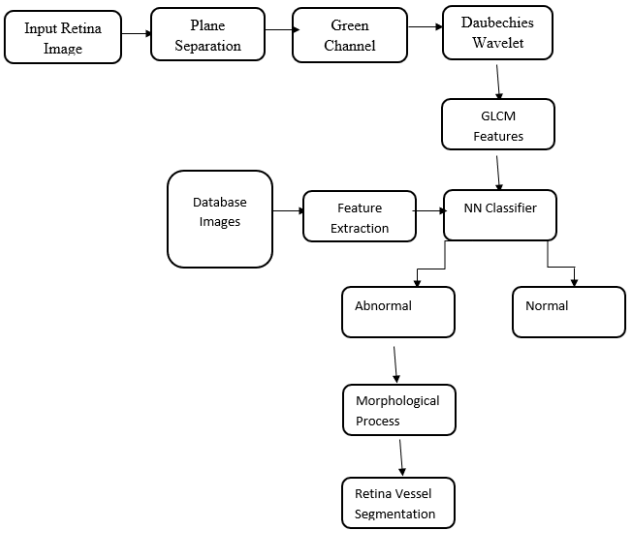

Fig. 7. Block diagram of the proposed system

(1) Enhancement: Blood vessels can be detected in retinal images via Kirsch's template. Fig. [8] in Kirsch's paper shows rotating templates in real time. One discrete variant of the first-order derivative is Kirsch's operator in the field of edge enhancement and detection. Detecting edges is done by rotating eight templates by 45 degrees successively. Kirsch operators work by detecting edge strengths along some predetermined directions, and are nonlinear algorithms

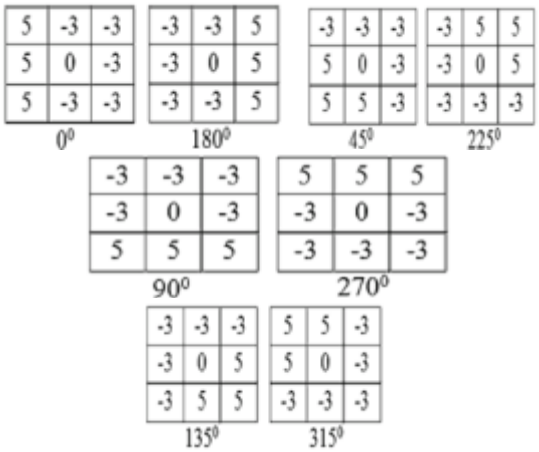

Fig. 8. 3x3 mask operators of kirsch templates

Gradients of different directions are achieved. Final gradients are created by adding up all the enhancements from the multiple RGB channels instead of considering a single channel alone. A grayscale image was produced from the edge-enhanced RGB image. The output grey image is I, and the red, green, and blue components are R, G, and B, respectively.

$$I=0.33R+0.5G+0.166B \quad (1)$$

(2) Image binarization/ plane separation: The grayscale based on the statistical histogram is 0 to L. A threshold of K is applied to the image to segment it into two classes: the background and the object. Gray-level is from 0 to grayscale based and the target whose Gray-level is from K+1 to L. If K is high enough, the value of interclass variance B can be the highest among all possible values. With K, target and background can be accurately separated. Foreground and background are assumed to be two separate classes of pixels in the image being thresholded, then the optimum threshold is calculated for separating the two classes with the minimum intra-class variance.

(3) Extracting the Green Component from the **RGB Image:** The red, green, and blue components of an RGB image are represented in a single m-by-n-by-3 array in MATLAB.[7] Three planes of red, green, and blue intensity values are represented by m and n, the row and column numbers of pixels in an image, respectively.

(4) Daubechies wavelet: Daubechies wavelet bases represent a set of orthonormal, compactly supported wavelet and scaling functions that are characterized by maximum regularity for a given length of the quadrature mirror filter support.

(5) Wavelet Transform:

The 1-D continuous wavelet transform is given by:

$$Wf(a,b) = \int_{-\infty}^{\infty} x(t)\ \psi_{a,b}(t)dt \quad (2)$$

The inverse 1-D wavelet transform is given by:

$$x(t) = \frac{1}{c}\int_{b=0}^{\infty}\int_{a=-\infty}^{\infty}\frac{1}{a^2}Wf(a,b)\psi_{a,b}(t)dbda \quad (3)$$

Where a - scaling parameter

b - shifting parameter, $\psi_{a,b}(t)$-mother wavelet

and $$C=\int_{-\infty}^{\infty}\frac{|\psi(\omega)|^2}{\omega}d\omega \quad (4)$$

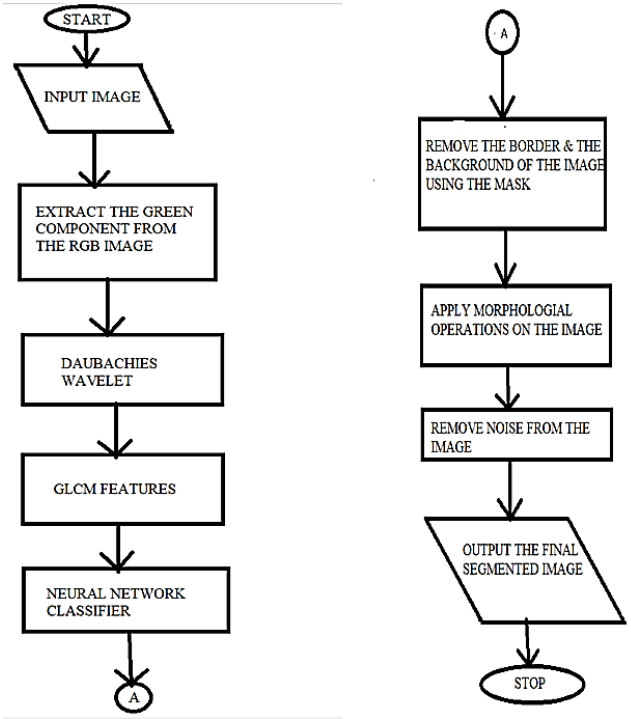

Fig. 9. Flow chart of the proposed method

$\psi(\omega)$ is the Fourier transform of the mother wavelet $\psi(t)$. C is required to be finite, which leads to one of the required properties of a mother wavelet. Since C must be finite, then $\psi(0) = 0$ to avoid a singularity in the integral, and thus $\psi(t)$must have zero mean.

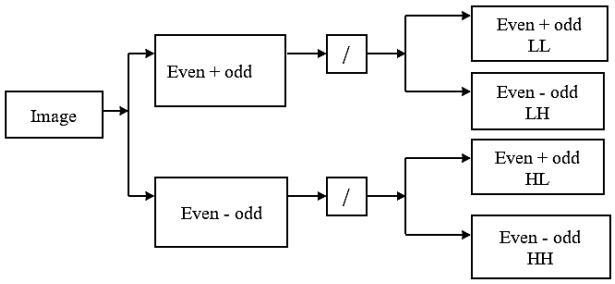

Fig. 10. Filter structure

3.1. Pixel Level Image Fusion

In the human visual system, the spatial frequency represents the active level of an image. Spatial frequency is defined by the following,

$$SF = RF^2 + CF^2 \tag{5}$$

The row frequency (RF) and column frequency (CF) of an 8x8 image block are given by,

$$RF^2 = \frac{1}{8x8}\sum_{x=0}^{7}\sum_{y=0}^{7}(f(x,y-(f(x,y-1)))^2$$

$$CF^2 = \frac{1}{8x8}\sum_{x=0}^{7}\sum_{y=0}^{7}(f(x,y-(f(x-1,y)))^2 \tag{6}$$

LDP stands for Local Directional Pattern in the world of image textures, which describes the spatial structure of an image texture in gray-scale. Based on the relative strength magnitude [14], All eight edge response values at each pixel point are computed using an LDP operator. Kirsch masks with eight orientations cantered on the position of [], 0,1,..,7m, i.e., are used to compute the edge response values of a central pixel in the image. In the Fig [11] below , the masks are depicted.

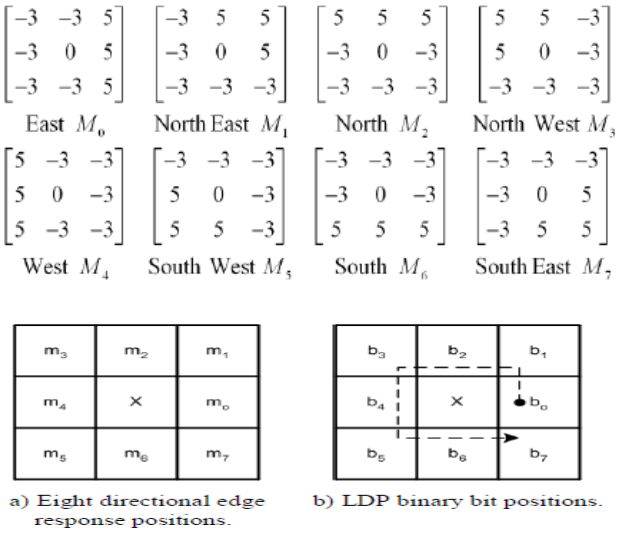

Fig. 11. Eight edge response values at each pixel point are computed using an LDP operator

Some orientations do not place the same emphasis on response values. Corners and edges are known to produce high response values [7]. Despite k top directional bit responses i b being set to one, the k most prominent directions to produce the LDP are mainly of significance here. In the 8-bit LDP pattern, the remaining (8-k) bits are set to 0. Using the equation above, we can derive the LDPcode. Denklemi buraya yazın.

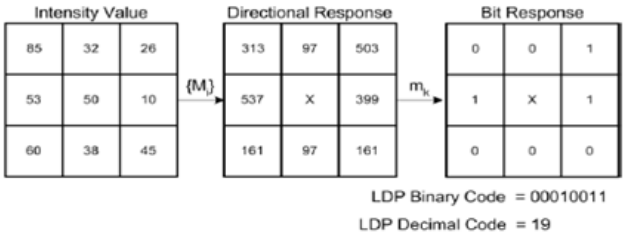

Fig. 12. The diagram shows the mask response of an illustration of how k=3 influences LDP bit placement

$$LDP_k = \sum_{i=0}^{7} b_i(m_i - m_k) \times 2^i \tag{7}$$

$$b_i(a) = \begin{cases} 1 & a \geq 0 \\ 1 & a < 0 \end{cases}$$

3.2. Parameter Evaluation

1) Peak –signal-to-noise ratio and Mean square error:

$$PSNR = 10*\log10\ (255*255/MSE) \tag{8}$$

The mean-squared difference between the cover picture and the stego-image is called MSE (Mean Square Error). In equation 3.9, the mathematical definition of MSE is as follows:

$$MSE = 1/(M*N)\ \sum_{i=1}^{M}\sum_{j=1}^{N}(aij\ - bij)^2 \tag{9}$$

The pixel value at location (i,j) in the input image is denoted by a_{ij}, and the pixel value at the same position in the output image is denoted by b_{ij}. For the quality assessment, PSNR is commonly calculated in decibels (dB). The higher the PSNR, the better the visual quality.

2) Entropy: It is useful to determine the significant information from the image based on the probability of pixel values.

$$S = -\sum_x \sum_y p(x,y) \log p(x,y) \tag{10}$$

Where, p (x, y) is the probability of each grey level.

3) Correlation Coefficient: It ensures that the original and rebuilt pictures have identical tiny structures [2]. More information is preserved when there is a higher correlation. In the space domain, the coefficient correlation is defined as:

Correlation = sum (sum (B.*A))/Sqrt (sum (sum (B.*A)) *sum (sum (A.*A))), Where B represents the difference between the fused picture and the overall mean value, and A represents the difference between these images and the overall mean value.

3.3. GLCM Features

The Gray Level Co-Occurrence Matrix (GLCM) is a statistical method to determine the second-order properties of an image based on its intensity points (pixels). There are G grey levels in a picture equal to the number of rows and columns in a GLCM matrix. A matrix element P (i, j) consists of the relative frequency of two pixels with (Δx, Δy).intensity 'i' and 'j' within a neighbourhood, separated by a pixel distance . The matrix element P (i, j | d, ɵ) contains the second-order statistical probability values for changes

between gray levels ‘i’ and ‘j’ at a particular displacement distance d and a particular angle (ɵ) [9]. Using a large number of intensity levels G implies storing a lot of temporary data, i.e., a G × G matrix for each combination of (Δx, Δy) or (d, ɵ). Since the GLCMs have a large dimensionality, their sensitivity to texture size is very high.

3.4. Neural Network Classifier

Artificial neural networks (ANNs) are models of neural networks that are a branch of artificial intelligence. With this model, patterns buried in data can be found quickly and precisely, thus replicating good knowledge. Data should be discovered continuously by AI systems [15]. Artificial intelligence technique is the most prevalent technique used in medical diagnosis relationships that have dissimilar data.

Specifically, an artificial neural network consists of many artificial neurons in a network in which they are linked together. In the process of creating significant outputs, neural networks convert inputs into significant outputs. A supervised or unsupervised teaching model can be used. Noise is necessary for neural networks to learn.

3.5. Morphological Process

An image that has small outlines or structures is evaluated using the morphological technique. When an image is structured, every pixel within a particular location is considered, and the pixels nearby that location are taken into account. Elements can be classified as fitting or not fitting into the neighborhood using one of several operations:[4]

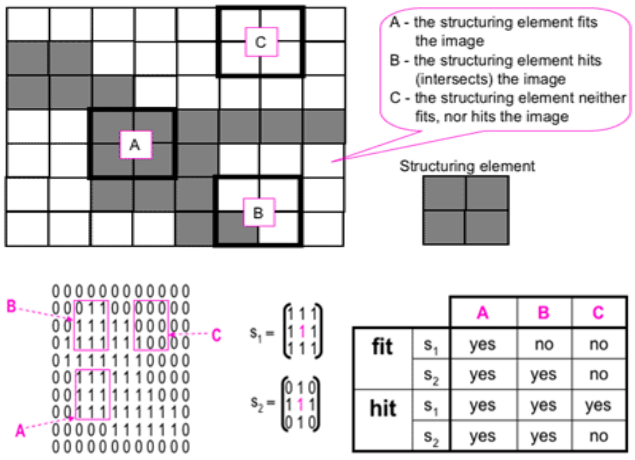

		A	B	C
fit	s_1	yes	no	no
	s_2	yes	yes	no
hit	s_1	yes	yes	yes
	s_2	yes	yes	no

Fig. 13. The testing of images with structuring elements

In this framework, the structuring element is a binary image, i.e. a set of pixels in which each pixel represents either a zero or a one [1]. Structure components are considered to fit an image when the associated image pixel is 1, in the same range of pixels as the structuring element. If, at a minimum, every related image pixel is set to 1, a structuring element is also considered to hit, or cross, an image.

The erosion of an image by using tiny square structuring elements (e.g., 2*2 - 5*5) removes pixels from the inner and outer borders of each region. In regions, there is an increase in hole size and omission of minor details. S1 and S2 are used to fit and hit the binary image. Dimensions and shape of a structuring element influence the dilation or erosion outcome. The dual process of dilation and erosion produces opposite results in that way. A complement of an image f is created when you replace one with zero or vice versa.

4. Simulation Results

The following results were observed under MATLAB version 2018 above. The epochs were kept at 100 after performing it at different values such as 40,60 which weren’t sufficient enough to detect the deep stage as shown in fig [17]. So, after increasing the epochs to 100 it was found that the error was minimized and accuracy was above 95%. The learning rate was 0.0001 for a normal eye and for an early-stage glaucoma. For moderate and deep cases, the learning rate were modified to 0.0002 and 0.0003. Also, the stage classification was performed and glaucoma stages were classified as normal, early, moderate, and deep.

Fig. 14. Result of an eye with glaucoma - Learning Rate:0.0002, Epochs:100, Stage Classification-Moderate

Fig.15. Result of an eye with glaucoma - Learning Rate:0.0001, Epochs:100, Stage Classification-Early

Fig. 16. Result of an eye no glaucoma - Learning Rate:0.0001, Epochs:100, Stage Classification-Normal

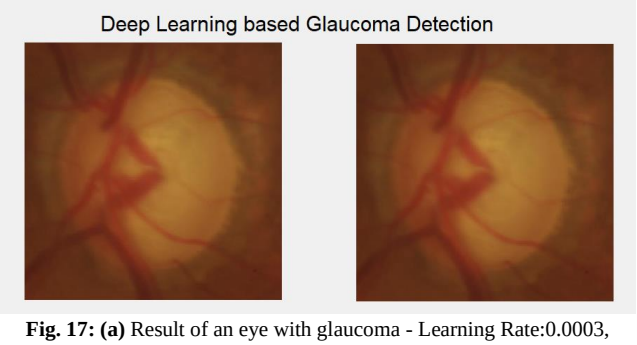

Fig. 17: (a) Result of an eye with glaucoma - Learning Rate:0.0003, Epochs:40, Stage Classification-Unclear and Deviated

Fig. 17. (b) Result of an eye with glaucoma - Learning Rate:0.0003, Epochs:60, Stage Classification (Detection)-Unclear and Deviated.

Fig. 17. (c) Result of an eye with glaucoma - Learning Rate:0.0003, Epochs:100, Stage Classification-Deep

5. Comparison

The comparison between the proposed algorithm and the existing method was performed and the above results were obtained. The proposed algorithm is highly accurate and has good sensitivity and specificity. Also, the time taken for detection is lesser than other existing algorithms. Fig [18] shows the results of implementing the proposed algorithm on 15 fundus images. The number of positive glaucoma cases is 13 out of 15. The early stage of glaucoma is detected in 4 cases and moderate is detected in 6, while 3 have deep stage glaucoma. The sensitivity and specificity are about 88%. The number of iterations were 40 and maximum epochs was 95.

Table 1. Comparison of methods

Methods	Sensitivity (%)	Specificity (%)	Learning rate	Accuracy (%)
Edge detection	85	87	0.05	92.3
Thresholding algorithm	98	100	0.003	94.11
Retinal grading algorithm	75.7	86	0.045	94.52
Deep Learning (Proposed)	88	89	0.0001	95.91

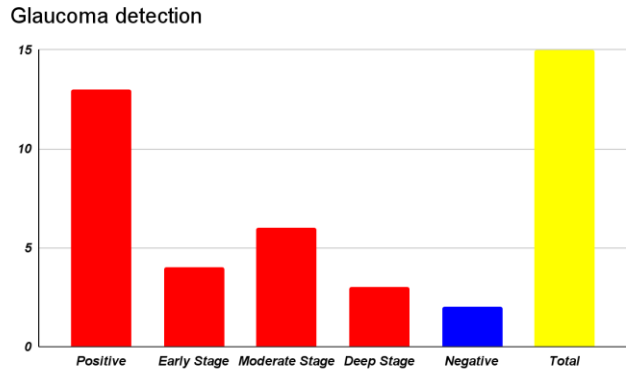

(a)

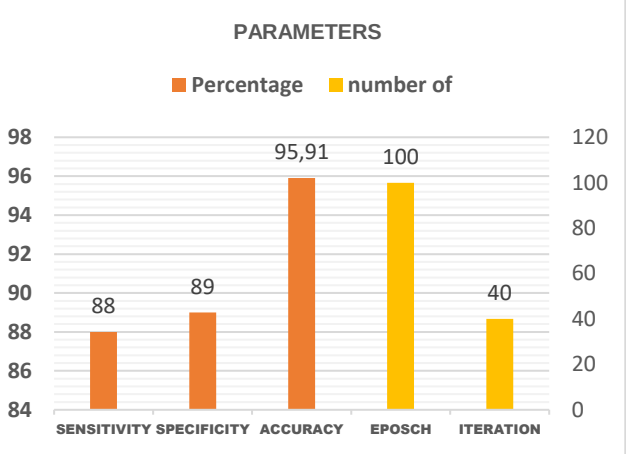

(b)

Fig.18. (a) and (b) results of implementing the proposed algorithm on 15 fundus images

6. Conclusion And Further Work

As long as the required features are segmented accurately, there will be accurate identification of the disease accompanied by a description of the stage of the disease or even the extent of the damage. R. The proposed algorithm performs well at early identification during the wavelet transformations and pixels-level fusion phases. As part of the proposed algorithm, Kirsch's template is used to extract the blood vessels, morphological closure is used to fill in the gaps around the blood vessels, and object classification is used to remove the unwanted parts. Based on findings, this approach was 95.9% accurate in glaucoma screenings. Consequently, this study may lead to automated screening systems for the early detection of glaucoma.

Further research will examine other parameters such as the retinal nerve, neuro-retinal area, and rim width of the retinal region that can be used as additional indicators of glaucoma progression. 3 D reconstruction methods can be used to determine the depths of progression. Furthermore, artificial intelligence techniques will be employed to find the appropriate parameters in several formulas, including wavelet-based approaches and threshold-based approaches.

References

[1] Philippe Salembier, “Structuring Element Adaptation for Morphological Filters”, Journal of Visual Communication and Image Representation, Volume 3, Issue 2, Pp. 115-136, June 1992.

[2] A. M. Mendonc¸a and A. Campilho, “Segmentation of retinal blood

vessels by combining the detection of centrelines and morphological reconstruction," IEEE *Trans. Med. Imag.*, vol. 25, no. 9, pp. 1200–1213,

[3] M. E. Martinez-Perez, A. D. Hughes, S. A. Thom, and K. H. Parker, "Improvement of a retinal blood vessel segmentation method using the insight segmentation and registration toolkit (ITK)," in *Proc. IEEE 29th Annu. Int. Conf. EMBS*. Lyon, IA, France, 2007, pp. 892–895.

[4] M. Lalonde, M. Beaulieu, and L. Gagnon, "Fast and robust optic disc detection using pyramidal decomposition and Hausdorff-based template matching," *IEEE Trans. Med. Imag.*, vol. 20, no. 11, pp. 1193–1200, Nov. 2001Sep. 2008.

[5] Youssif, A.A.-H.A.-R., Ghalwash, A.Z., Ghoneim, A.A.S.A.-R.: Optic disc detection from normalized digital fundus images employing a vessels' direction matched filter. IEEE Transactions on Medical Imaging 27, 11–18 (2008)

[6] T. Kauppi and H. Kälviäinen, "Simple and robust optic disc localization using the decorrelated templates," in *Proc. 10th Int. Conf. Advanced Concepts for Intel. Vision Syst.*, Berlin, Germany: Springer-Verlag, 2008, pp. 719–729.

[7] Banerjee, B., Bhattacharjee, T., Chowdhury, N.: Colour Image Segmentation Technique Using Natural Grouping of Pixels. International Journal of Image Processing (IJIP) 4(4), 320–328 (2010)

[8] Mohamed Saleem TS, Jain A, Tarani P, Ravi V, Gauthaman K. "Aliskiren: A Novel, Orally Active Renin Inhibitor." Systematic Reviews in Pharmacy 1.1 (2010), 93-98. Print. doi:10.4103/0975-8453.59518

[9] Rajendra Acharya, et al, (2011). Automated Diagnosis of Glaucoma Using Texture and Higher-Order Spectral Features. IEEE Transactions on information technology in biomedicine. 15(3):449-455.

[10] Jyotiprava Dash and Nilamani Bhoi. A thresholding-based technique to extract retinal blood vessels from fundus images. Future Computing and Informatics Journal, 2(2):103–109, 2017.

[11] Huazhu Fu, Jun Cheng and Yanwu Xu. Disc-aware Ensemble Network for Glaucoma Screening from Fundus Image. In 2017 an IEEE transaction Journal on medical imaging, 2017.

[12] Alreja, G., Lotfi, A. Eustachian valve endocarditis: Rare case reports and review of the literature (2011) Journal of Cardiovascular Disease Research, 2 (3), pp. 181-185. DOI: 10.4103/0975-3583.85266

[13] Ganesh E., Member, IEEE, Shanker N.R., and Priya.M. Non-Invasive measurement of glaucoma disease at an earlier stage through GMR sensor AH bio-magnetic signal from the eye and RAWDT algorithm. In 2018, an IEEE journal, 2018.

[14] S. S. Kanse and D. M. Yadav. Retinal fundus image for glaucoma detection: A review and study. Journal of Intelligent Systems, 28(1):43– 56, 2017.

[15] Bhupendra Singh Kirar, Dheeraj Kumar Agrawal. Computer-aided diagnosis of glaucoma using discrete and empirical wavelet transform from fundus images. In 2018 an IET image process journal at Maulana Azad National Institute of Technology, Bhopal, India, 2018.

[16] Diaz-Pinto, A. Morales, S., Naranjo, V. *et al.* CNNs for automatic glaucoma assessment using fundus images: an extensive validation. *BioMed Eng Online* 18, 29 (2019)